Multicompartment duct platform to study epithelial–endothelial crosstalk associated with lung adenocarcinoma

Cite as: APL Bioeng. 8, 026126 (2024); doi: 10.1063/5.0207228
Submitted: 6 March 2024 · Accepted: 24 May 2024 ·
Published Online: 17 June 2024

Keith A. Gagnon,[1,2] Jessie Huang,[3,4] Olivia T. Hix,[3,4] Veronica W. Hui,[1] Anne Hinds,[4] Esther Bullitt,[5] Jeroen Eyckmans,[1,2,6] Darrell N. Kotton,[3,4,a)] and Christopher S. Chen[1,2,6,a)]

AFFILIATIONS

[1]Department of Biomedical Engineering, Boston University, Boston, Massachusetts 02215, USA
[2]Biological Design Center, Boston University, Boston, Massachusetts 02215, USA
[3]Center for Regenerative Medicine (CReM), Boston University and Boston Medical Center, Boston, Massachusetts 02118, USA
[4]The Pulmonary Center and Department of Medicine, Boston University Chobian & Avedisian School of Medicine, Boston, Massachusetts 02118, USA
[5]Department of Pharmacology, Physiology & Biophysics, Boston University Chobian & Avedisian School of Medicine, Boston, Massachusetts 02118, USA
[6]Wyss Institute for Biologically Inspired Engineering, Harvard University, Boston, Massachusetts 02215, USA

[a)]**Authors to whom correspondence should be addressed:** dkotton@bu.edu and chencs@bu.edu

ABSTRACT

Previous lung-on-chip devices have facilitated significant advances in our understanding of lung biology and pathology. Here, we describe a novel lung-on-a-chip model in which human induced pluripotent stem cell-derived alveolar epithelial type II cells (iAT2s) form polarized duct-like lumens alongside engineered perfused vessels lined with human umbilical vein endothelium, all within a 3D, physiologically relevant microenvironment. Using this model, we investigated the morphologic and signaling consequences of the $KRAS^{G12D}$ mutation, a commonly identified oncogene in human lung adenocarcinoma (LUAD). We show that expression of the mutant $KRAS^{G12D}$ isoform in iAT2s leads to a hyperproliferative response and morphologic dysregulation in the epithelial monolayer. Interestingly, the mutant epithelia also drive an angiogenic response in the adjacent vasculature that is mediated by enhanced secretion of the pro-angiogenic factor soluble uPAR. These results demonstrate the functionality of a multi-cellular *in vitro* platform capable of modeling mutation-specific behavioral and signaling changes associated with lung adenocarcinoma.

I. INTRODUCTION

Lung cancer is the leading cause of cancer-associated mortality in the United States.[1] Among histological subtypes, lung adenocarcinoma (LUAD), a type of non-small cell lung cancer, is the most common type of lung cancer, accounting for nearly 40% of all cases. Due to its aggressive nature and frequent discovery late in disease course, the median survival of LUAD is less than five years from diagnosis.[2] Alveolar epithelial type II (AT2) cells, which are responsible for surfactant production and regeneration of the alveolar epithelium following injury, have recently been identified as the cell of origin for LUAD.[3,4] Unfortunately, these cells are challenging to obtain from patients, particularly at early stages of disease and difficult to maintain in culture, as these cells tend to lose their AT2 program with serial passaging.[5] Historically, these traits have made *in vitro* investigation into the origins of LUAD difficult, and as such, our understanding of the pathogenesis and mechanisms of metastasis of LUAD remains limited.[5–7]

Over the last decade, organ-on-chip models have enabled the mechanistic study of fundamental biological processes with high spatiotemporal precision and led to significant advances in our understanding of lung biology and pathology. Mechanically actuated devices have been used to demonstrate the role of strain on drug transport, tumor growth, tissue repair, and epithelial permeability.[8–11] Others have focused on the development of multi-cellular co-culture devices, including co-culture of primary bronchial epithelium with primary

microvascular endothelial cells, as well as co-culture of immortalized lung cancer cells with vasculature.[12,13]

While these devices have significantly improved our understanding of lung pathology, most have relied on immortalized human lung epithelial cell lines, which diverge in phenotype and function from native alveolar epithelium. Numerous studies have demonstrated that immortalized lines, such as A549, lose expression of the gene regulatory networks that define human AT2 cells and consequently differ significantly in terms of response to infection, morphology, and ability to produce surfactants.[14–17] Additionally, many of these devices culture cells directly on a PDMS/polymeric membrane of supraphysiologic stiffness and porosity, with largely planar rather than tubular surfaces, all features that are known to alter cellular organization and function.[18–23] Furthermore, there is a need to expand from single-lineage 3D models to more complex multi-lineage human models, where crosstalk between multiple cell types derived from various germ layers can be examined in otherwise difficult-to-access platforms, such as modeling the epithelial–endothelial interactions that drive LUAD progression.[24] However, achieving this level of complexity requires a platform that enables *a priori* control of tissue structure, identification of compatible media able to support the co-existence of different cell lineages, and tools for achieving precise spatiotemporal control of genes for disease modeling.

To address these challenges, we have developed a novel lung-on-a-chip platform in which we are able to co-culture human iPSC-derived AT2 cells (iAT2s) with primary human endothelial cells in distinct channels within an extracellular matrix-based hydrogel with physiologically relevant geometries. iAT2s have previously been shown to functionally and transcriptionally mirror native AT2 cells, while maintaining the ability to proliferate indefinitely.[25,26] These cells have also shown promise in modeling behavioral consequences of expression of LUAD-related oncogenes, as iAT2s genetically modified to conditionally express $KRAS^{G12D}$, a common oncogenic mutation implicated in the development of lung adenocarcinoma,[27,28] were recently shown to have increased proliferation and reduction in AT2 phenotype in an organoid model.[29] Kirsten rat sarcoma virus (KRAS) is the most frequently mutated oncogene in cancer, and the codon 12 activating mutation, $KRAS^{G12D}$, is one of the most prevalent KRAS mutations in all carcinomas.[30] In LUAD, the $KRAS^{G12D}$ mutation defines a subset of patients associated with a lower pack-year smoking history, lower tumor mutational burden, and distinct clinical and immunologic features compared to non-G12D mutations.[31] Thus, $KRAS^{G12D}$ is an essential KRAS mutation to study due to its prominence in lung adenocarcinoma patients, as well as its distinct characteristics that necessitate targeted therapy.

Here, incorporation of conditionally expressing $KRAS^{G12D}$ iAT2s into our 3D microfluidic platform enabled on-chip modeling of the biological consequences of $KRAS^{G12D}$-mediated LUAD in terms of both epithelial morphology and response of nearby vascular endothelium. Using this model, we demonstrate that epithelial $KRAS^{G12D}$ expression led to a lumen-filling hypercellularity coupled with disrupted epithelial morphology and demonstrate alterations in paracrine crosstalk that ultimately drive an angiogenic response in the adjacent engineered vessel. We show that these changes are mediated, in part, through enhanced secretion of soluble urokinase-type plasminogen activator receptor (suPAR). We anticipate that the high spatiotemporal resolution of 3D morphodynamic remodeling afforded by this model system will enable additional mechanistic studies of lung epithelial–endothelial interactions in development, disease, and drug testing contexts.

II. RESULTS

A. iPSC-derived alveolar epithelial type 2 cells maintain identity in the EpiChip

The EpiChip is a PDMS-based microfluidic device designed with a blunt ended duct adjacent to an endothelialized conduit in a 3D extracellular matrix (ECM) microenvironment, functionally enabling the development of a terminal epithelial duct with central lumen adjacent to a perfused, engineered vessel [Fig. 1(a)].[32] Disaggregation of iAT2 alveolospheres (N = 3 iPSC lines: SPC2-ST-B2, BU3 NGST, and BU3 NGST KRAS3) and seeding of the blunt-ended epithelial duct with a cell suspension of iAT2s enabled the generation of iAT2-seeded ducts [Figs. 1(b) and 1(a), supplementary material]. Over the span of five days in a chemically defined serum-free, feeder-free medium,[26] iAT2s were able to form a peripheral cuboidal epithelial monolayer around a central lumen, while maintaining expression of $SFTPC^{tdTomato}$, indicating maintenance of AT2 identity [Fig. 1(b)]. As alveolosphere cultures are typically grown in 3D Matrigel™ (MG) for 12–14 days before passaging, we anticipated that a MG coating of the epithelial duct would improve cellular adhesion and growth.[26,33] As predicted, MG coating of the duct increased cellular adhesion and promoted the development of a confluent monolayer at earlier time points [Fig. 1(b), supplementary material].

We next tested whether EpiChip culture alters iAT2 morphology, polarity, or function as compared to alveolosphere culture in 3D MG. To do so, we stained for junctional markers, including E-cadherin, EpCAM, and the proliferative marker Ki67 using immunofluorescence. iAT2s in typical 3D culture expressed basolateral, cup-like EpCAM and E-cadherin and included a subset of proliferating cells [Fig. 1(c), left]. iAT2s cultured within the epithelial duct of the EpiChip showed similar basolaterally localized cell adhesion molecules [Fig. 1(c), right]. In contrast to iAT2s in 3D MG culture, iAT2s in the EpiChip assumed a quiescent phenotype typical of resting human AT2 cells, evident as reduced Ki67 staining in the monolayer covering the epithelial duct [Fig. 1(c)].

As apicobasal polarization and production of surfactant-containing lamellar bodies are both necessary for appropriate biological function of AT2 cells, we next assessed iAT2 ultrastructure following formation and maintenance of a contiguous monolayered epithelium in the EpiChip. Using transmission electron microscopy (TEM), we observed apical microvilli facing into the epithelial duct lumens and lamellar body formation with localization to the apical surface of iAT2s in the EpiChip. Electron dense projection cores appeared within most lamellar bodies [Figs. 1(d) and 1(c), supplementary material], as has been described previously for human but not rodent primary AT2 cells.[34] These hallmark ultrastructural features of AT2 cells, in addition to the basolateral, cup-like EpCAM, and E-cadherin localization by immunofluorescence microscopy [Fig. 1(c)], suggest both the maintenance of AT2 identity and appropriate apicobasal polarization of the iAT2s in the EpiChip. We observed no loss of AT2 identity in our samples, specifically, no AT2 transdifferentiation to flat alveolar epithelial type 1 cells (AT1) as endogenous AT2s are capable of doing.[35] This phenotype maintenance was expected due to

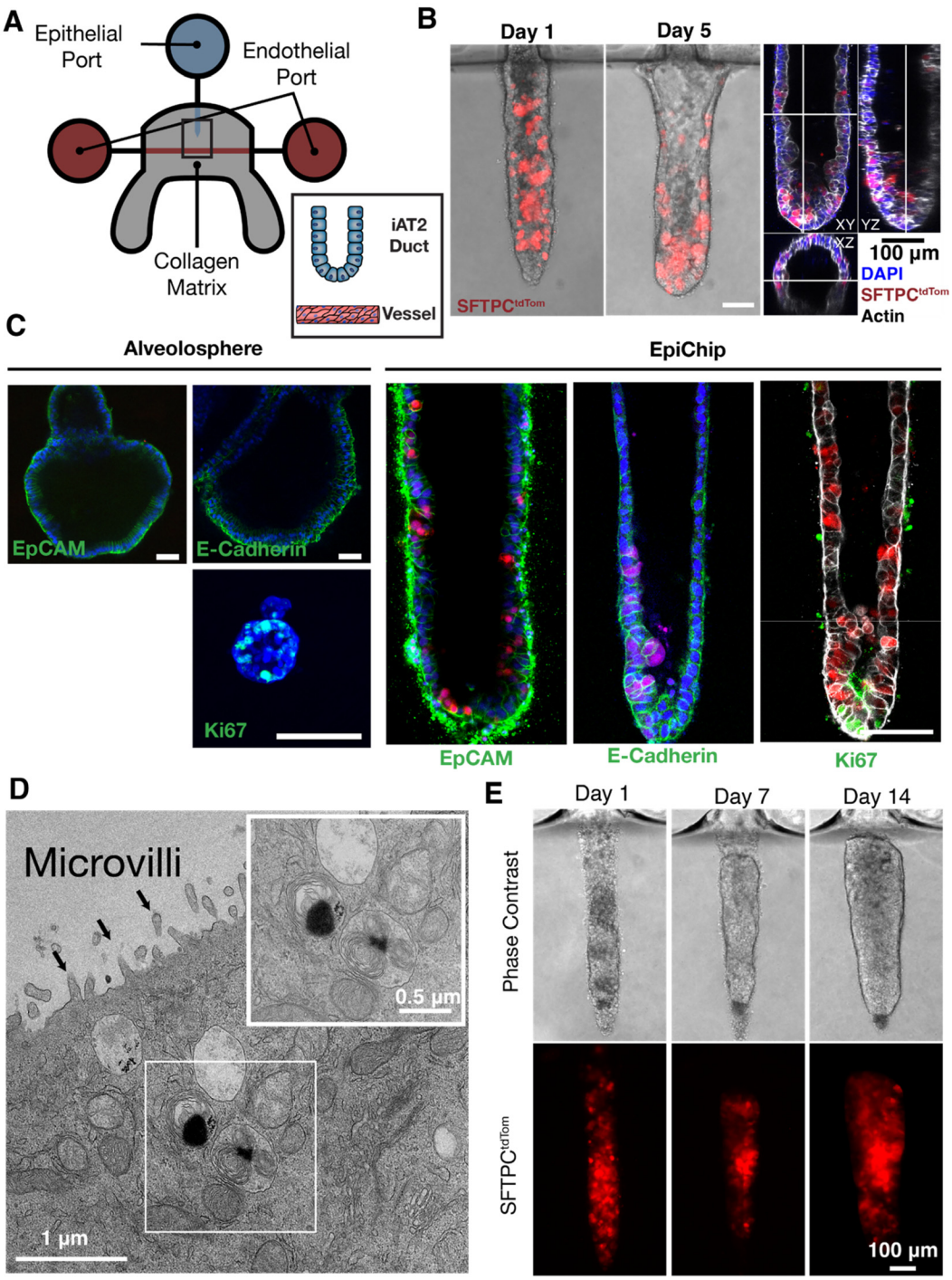

FIG. 1. iPSC-derived alveolar epithelial type 2 cells maintain identity in the EpiChip. (a) Schematic of the EpiChip device, depicting a blunt ended epithelial duct, perfusable endothelial duct, and collagen matrix region. The inset shows cellular architecture within the collagen matrix. (b) iAT2s seeded into the epithelial duct adhere to MG-coated collagen duct and ultimately form a peripheral monolayer surrounding a centralized lumen. (c) iAT2s in the alveolosphere culture show basolateral E-Cad and EpCAM expression with a subset of proliferating cells (Ki67) (left, scale = 50 μm). iAT2s seeded into the EpiChip show similar basolateral E-Cad and EpCAM staining but relative growth arrest (right, scale = 100 μm, Blue: DAPI; Green: Specified Molecule; Red: SFTPC^{tdTom,} Gray: Actin) (d) TEM of iAT2 cells forming the peripheral monolayer exhibits apicobasal polarization with apical microvilli facing the EpiChip lumen and ultrastructural features typical of human AT2 cells such as multivesicular bodies and lamellar bodies with electron dense projection cores (inset). (e) iAT2 ducts can be cultured for at least 14 days in the EpiChip and maintain expression of SFTPC^{tdTom} expression.

maintenance of cells in a medium optimized to sustain the AT2 phenotype.

Although the detection of lamellar bodies by TEM, basolateral EpCAM expression, and sustained SFTPC^{tdTomato} expression suggest maintenance of type 2 cell identity over the course of our 5 day experiments, we sought to test the stability of this phenotype within the EpiChip. Prolonged culture of iAT2 cells in the EpiChip demonstrated sustained expression of SFTPC^{tdTomato} over 14 days in culture, again suggesting that culture of these cells in the EpiChip does not affect AT2 identity [Fig. 1(e)]. Collectively, these results suggest that iAT2 cells in the EpiChip can form a lumenized, quiescent peripheral monolayer with similar morphology and polarization to iAT2 in 3D MG culture and sustained maintenance of AT2 identity.

B. Supplementation of iAT2 medium with bFGF and VEGF supports iAT2-HUVEC co-culture

To investigate epithelial–endothelial interactions in the EpiChip, a common medium that could support both iAT2s and HUVECs was required. iAT2s are known to show a loss of AT2 phenotype when exposed to serum,[26] a common and often necessary element in endothelial media, so we searched for compatible media based on the native serum-free iAT2 medium, CKDCI, so named for its constituent components: CHIR99021, KGF, Dexamethasone, 8-Br-cAMP and IBMX. Cellular viability and function were tested in various combinations of CKDCI and EGM2, the native HUVEC medium. Both cell types were cultured in EGM2, CKDCI, a 1:1 blend of CKCDI and EGM2, and CKDCI + VEGFA + bFGF, two growth factors known to be important in endothelial survival.[36] Representative images and quantification of number of adherent HUVECs after 5 days of culture in each medium, are shown in Figs. 2(a) and 2(b). HUVECs maintained strong VE-Cadherin junctions and did not show significant loss of number of adherent cells when cultured in their native EGM2 medium, a 1:1 blend of CKDCI and EGM2 or CKDCI + VEGFA + bFGF (hereafter termed "CKDCI++"); however, a significant loss in cell number was seen in CKDCI alone, suggesting poor medium compatibility with HUVECs.

Flow cytometry was used to assess iAT2 performance in alveolospheres cultured in each medium. Analysis of NKX2-1^{GFP} and SFTPC^{tdTomato} reporters targeted to their endogenous human loci, respectively, demonstrated that NKX2-1^{GFP}, a pan-epithelial lung lineage marker, was significantly diminished in EGM2 culture, and SFTPC^{tdTomato}, a specific marker of AT2 cell identity, was significantly reduced in the 1:1 blend and EGM2-alone media. Importantly, NKX2-1^{GFP} and SFTPC^{tdTomato} co-expression was maintained in iAT2s cultured in CKDCI++ medium, suggesting that this medium can support iAT2 identity for at least 5 days, the duration of the assay [Figs. 2(c) and 2(d)]. Similar results were seen at the transcript level by RT-qPCR analysis of iAT2s in each of the media conditions [Fig. 2(e)]. Collectively, these results demonstrate that CKDCI++ can support both iAT2s and HUVECs, independently, suggesting that it could serve as a common medium to permit co-culture experiments.

To ensure that sustained culture in CKDCI++ would not adversely affect 3D endothelial vessels, HUVEC vessels were generated within the endothelial compartment of the EpiChip and cultured for five days in each specified medium. Staining for VE-cadherin suggests that endothelial cells can establish mature VE-cadherin junctions when cultured in CKDCI++, but not CKDCI [Fig. 2(f)]. Similarly, culture of iAT2 ducts in the EpiChip in CKDCI++ did not adversely affect their duct-forming abilities or their basolateral localization of EpCAM [Fig. 2(a), supplementary material]. These data confirm that CKDCI++ can support both cell types in a 3D collagen microenvironment, further suggesting that CKDCI++ could permit co-culture experiments within the EpiChip.

Morphologically, HUVEC vessels cultured in CKDCI++ were noted to have a larger diameter than vessels cultured in their native EGM2 medium. We anticipated that this was a physiologically relevant response of the endothelium to the 8-Br-cAMP and IBMX in the CKDCI medium, which act to raise intracellular cAMP levels, functionally reducing cytoskeletal tension and leading to increased diameter of the engineered vessel.[37] To test this, engineered vessels were cultured in the EpiChip for two days in their normal EGM2 media, and then switched to either CKDCI++ or CKD++ (omitting 8-Br-cAMP and IBMX). While the vessels switched to CKDCI++ showed immediate dilation, those switched to CKD++ did not have any significant changes in vessel diameter over the three additional days of culture, suggesting that the dilation is secondary to cAMP-mediated increases in vessel diameter, a physiologically relevant response within the endothelium [Fig. 2(b), supplementary material]. This result demonstrates that the endothelium still responds to physiologically relevant cues even when cultured in the modified iAT2/HUVEC medium, further identifying this medium blend as a viable medium for sustained iAT2/HUVEC co-culture.

To test the ability of CKDCI++ to support both cell types when cultured together, iAT2 and HUVECs were seeded into the epithelial and the endothelial ports of the EpiChip, respectively, and co-cultured in CKDCI++ for 5 days. Both phase contrast and immunofluorescence microscopy indicated normal junctional protein localization and cell morphology of both cell types, with clear junctional VE-cadherin localization in the lumenized HUVEC vessel and a clear peripheral monolayer around a central lumen in the iAT2 epithelium [Fig. 2(g)]. Together, these results suggest that CKDCI++ medium can support both iAT2 and HUVECs in the EpiChip for at least 5 days, facilitating further investigation of iAT2/HUVEC interactions in physiologically relevant microdevices.

C. KRAS^{G12D} mutation drives a change in iAT2 morphology secondary to increased proliferation

Understanding the consequences of distinct and recurring driver mutations in lung adenocarcinoma (LUAD) has been difficult, as few humanized models exist to study their behavior in cultures that recapitulate aspects of the native 3D microenvironment. As the EpiChip permits high spatiotemporal monitoring of key morphologic events and paracrine interactions between epithelial and endothelial compartments, we next turned to modeling the early stages of LUAD in this device. To do so, we utilized our BU3 NGST-TetOn:KRASG12D reporter iPSC line engineered to carry NKX2-1^{GFP} and SFTPC^{tdTomato} reporters as well as a doxycycline (dox)-inducible KRAS^{G12D} oncogene targeted to the AAVS1 locus [Fig. 3(a)].[29] We generated iAT2s from this iPSC line and treated parallel wells of the resulting iAT2s with either dox or DMSO vehicle control in 3D alveolosphere culture [Fig. 3(b)]. As expected, dox treatment induced expression of *KRAS* accompanied by a significant decrease in *SFTPC* expression, consistent with our previously published observation that KRAS^{G12D} promotes a shift in both primary and iPSC-derived AT2s away from a mature state

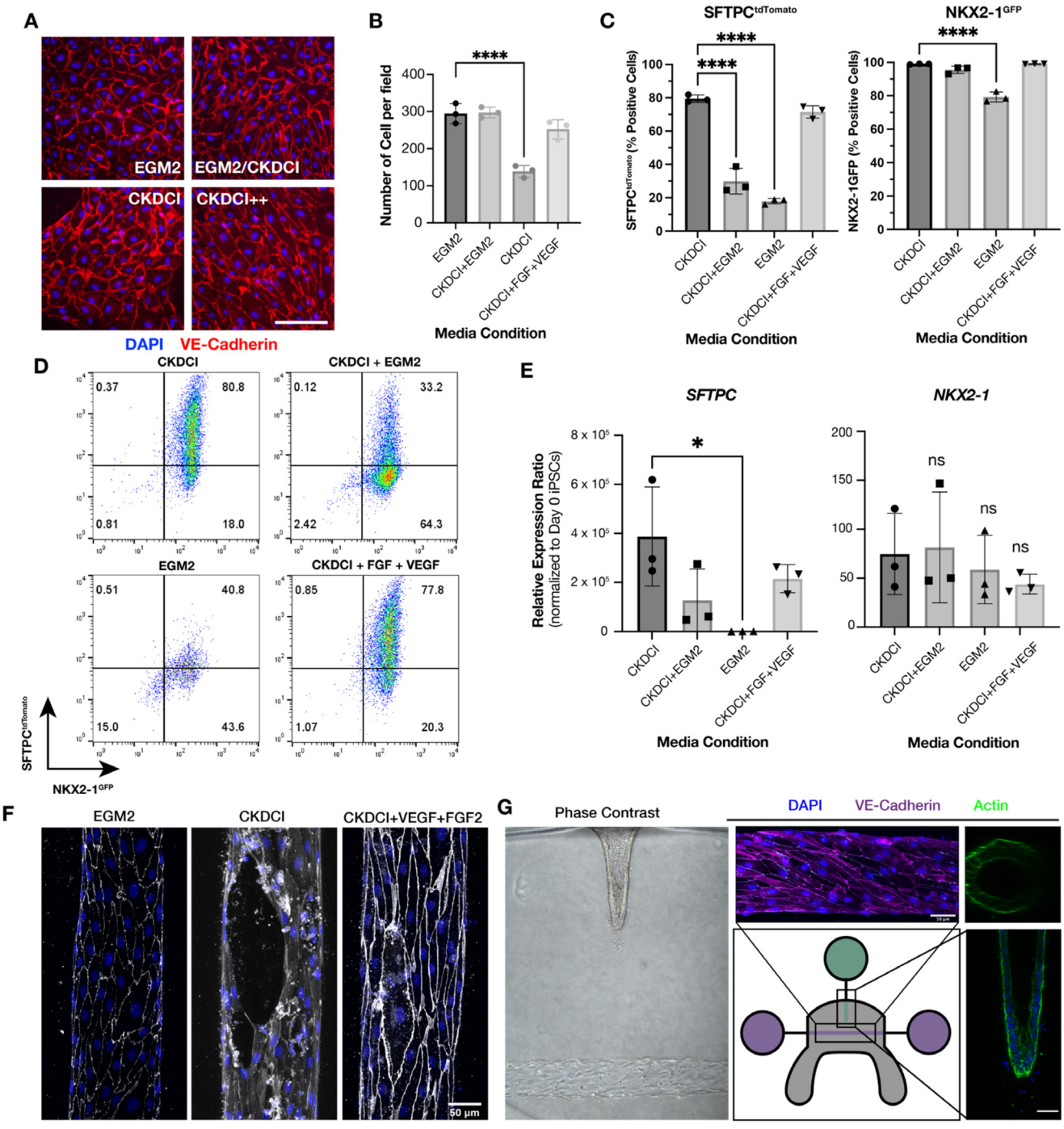

FIG. 2. CKDCI++ supports iAT2/endothelial co-culture in EpiChip. (a) Representative images of 2D monolayers of HUVECs cultured for 5 days in either EGM2, CKDCI, 1:1 blend of EGM2/CKDCI, or CKDCI + VEGFA + bFGF (CKDCI++). Red = VE-cadherin, Blue = DAPI. (b) Number of remaining adherent HUVECs in each condition after 5d of co-culture in each medium. (c) Percentage (by FACS) of iAT2 cells expressing $SFTPC^{tdTomato}$ (left) or $NKX2\text{-}1^{GFP}$ (right) after 5d culture in each indicated medium. (d) Representative FACS plots showing expression of $NKX2\text{-}1^{GFP}$ and $SFTPC^{tdTom}$ in each media. (e) RT-qPCR analysis of *SFTPC* (left) and *NKX2-1* (right) mRNA expression in iAT2 cells after 5 days culture in each medium (each point is an individual well). (f) HUVEC vessel micrographs stained for VE-cadherin after 5d of culture in each listed medium. (g) Phase contrast image of iAT2s and HUVECs in EpiChip after 5d (left), maximum projection of VE-Cadherin stained endothelial duct (upper middle), and XZ cross-sectional confocal micrograph of actin-stained iAT2 seeded epithelial duct (top right) and confocal micrograph of a single slice of an iAT2 seeded epithelial duct, all after 5d co-culture. (* $p < 0.05$, **** $p < 0.0001$).

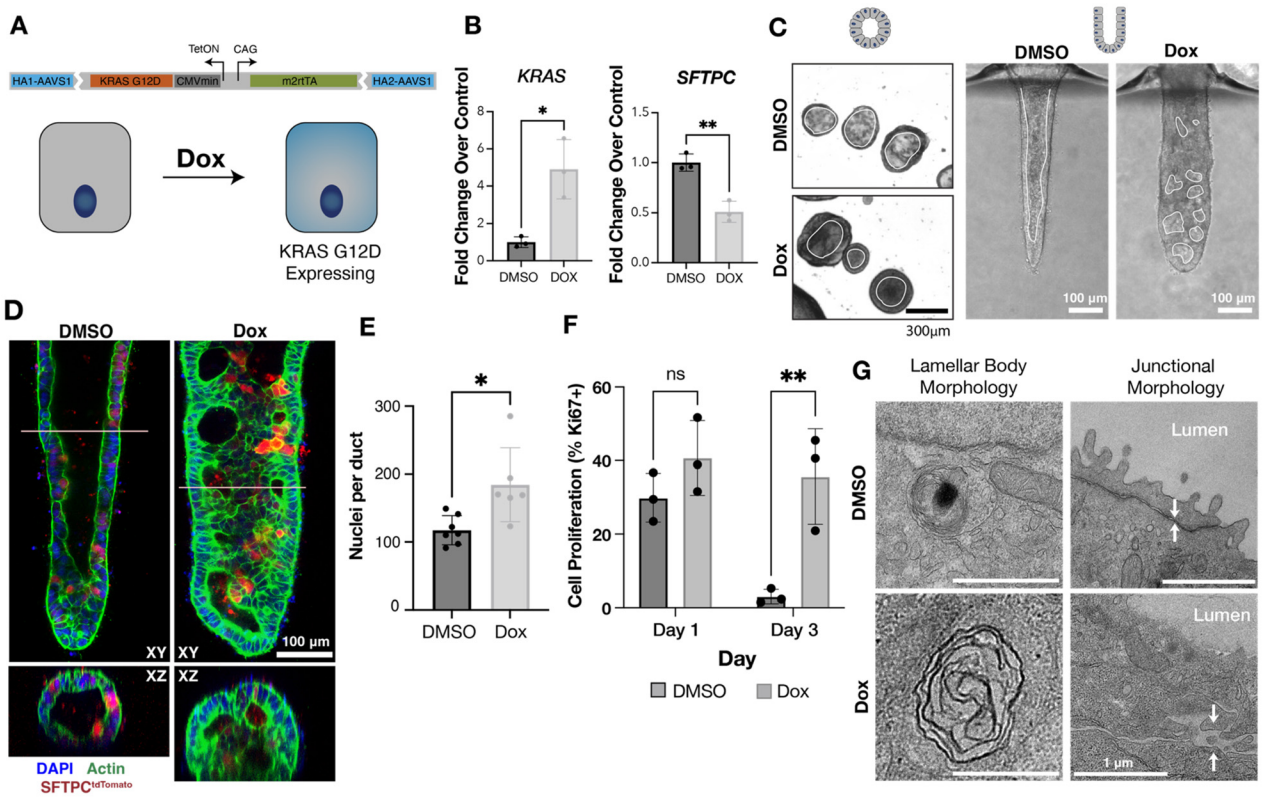

FIG. 3. KRAS^{G12D} expression drives a change in epithelial morphology secondary to increased iAT2 proliferation. (a) Schematic of the dox-inducible KRAS^{G12D} cassette knocked into the AAVS1 locus of BU3 NGST-TetOn:KRASG12D iPSCs. (b) RT-qPCR data showing an increase in *KRAS* expression in dox-induced cells and a decrease in *SFTPC* expression. (c) Phase contrast images of DMSO and dox-treated alveolospheres (left) and EpiChip ducts (right). White outlines indicate acellular lumen or luminal pockets. (d) Immunofluorescent micrograph (and XZ cross sections) contrasting the morphology of ducts seeded with DMSO-treated iAT2s vs dox-treated iAT2s expressing KRAS^{G12D}. (e) Number of cells (including peripheral monolayer and luminal cells) counted in mid-plane sections of ducts. (f) Quantification of proliferation, scored by fraction Ki67+ cells, in DMSO- vs dox-treated devices at 1d and 3d post seeding. (g) TEM images comparing lamellar bodies (left) and apical tight junctions (right) in DMSO and dox-treated iAT2s in EpiChip devices. (* $p < 0.05$, ** $p < 0.01$).

into a more proliferative AT2 progenitor cell state.[29] The inducible nature of these cells, together with their fluorescent reporter readouts, make them useful for the investigation of oncogenic behavioral changes in AT2-like cells in our co-culture model system.

As oncogene expression can drive significant morphologic and proliferative changes in epithelial cells, we next examined the morphology of ducts seeded with iAT2s harboring the KRAS^{G12D} alteration. While dox-treated iAT2s maintain luminal alveolosphere morphology in 3D alveolosphere cultures as we previously reported, an altered morphology emerged when dox-treated iAT2 cells were seeded into the epithelial duct of the EpiChip [Fig. 3(c)].[29] In contrast to the peripheral monolayer and large central lumen seen in the DMSO-treated cells, ducts seeded with dox-treated iAT2s exhibited significant hypercellularity and luminal infilling that reduced the central lumen to several smaller, disconnected acellular pockets [Fig. 3(d)]. Daily imaging of these ducts suggested that this infilled phenotype emerges early in the dox-treated ducts, with acellular pockets in the hypercellular central region clearly visible by day three of culture [Fig. 2(c), supplementary material]. Quantification of the number of cells in a mid-duct confocal slice of each sample demonstrated that ducts harboring dox-treated iAT2s had significantly more cells, consistent with the hypercellular phenotype seen in these ducts [Fig. 3(e)].

To assess if this increased number of cells was the result of increased proliferation, an expected response to constitutive KRAS activity, ducts were fixed at one- and three-days post seeding and stained with Ki67 to determine the number of cells in S-phase of the cell cycle.[38,39] At one day post seeding, there were no statistically significant differences in the fraction of proliferating cells in DMSO- and dox-treated ducts. However, by 3 days post seeding, dox-treated ducts showed clear maintenance of proliferation, while DMSO-treated ducts showed a significant reduction in fraction of proliferating cells [Fig. 3(f)]. This response is consistent with the expected quiescent phenotype of normal iAT2s after sufficient seeding and outgrowth, as observed in Fig. 1. These results suggest that both cell lines undergo an initial proliferative burst as they establish a confluent peripheral monolayer, with growth arrest by day three in the DMSO-treated cells but continued proliferation and expansion in the KRAS^{G12D} expressing iAT2s. These findings are consistent with the hyperplasia observed in multiple KRAS^{G12D} models, including primary mouse and human

AT2s, further validating that culture in this platform does not significantly alter key behavioral responses of AT2.[29,40,41]

Ultrastructural comparison of DMSO and dox-treated ducts suggested that KRAS^{G12D} expressing iAT2s have significantly fewer lamellar bodies. In fact, in contrast with normal or DMSO treated iAT2s, where multiple lamellar bodies were observed [Figs. 1 and 3(g)], only a single, albeit dysmorphic lamellar-like body, indicative of a single functionally mature iAT2 cell, could be found in tissue sections of ducts seeded with dox-exposed KRAS^{G12D} iAT2s [Fig. 3(g)], a finding in line with our prior report that KRAS^{G12D} drives a less mature, more progenitor-like state in iAT2s.[29] Furthermore, while the apical tight junctions between DMSO-treated iAT2s were narrow with closely abutting cell membranes as expected for an intact epithelial barrier, junctions between dox-treated expressing cells showed significant disruption [Fig. 3(g)]. These data suggest KRAS^{G12D} iAT2s exhibit altered, dysregulated morphology and growth in the EpiChip.

D. KRAS^{G12D}-expressing iAT2s drive an angiogenic response in adjacent vessels partially mediated by epithelium-secreted uPAR

One of the quintessential hallmarks of cancer is the ability of a tumor to promote angiogenesis in nearby vasculature.[42] While expression of a single oncogene does not entirely recapitulate the multitude of cellular changes that occur in carcinogenesis, the behavioral changes associated with expression of an oncogene can contribute to increased angiogeneic signaling from the cells harboring the mutation. Thus, we next investigated the impact of the KRAS^{G12D} oncogenic mutation in iAT2 cells on nearby endothelial cells to assess the role of this oncogene in tumor angiogenesis. To this aim, we co-cultured either DMSO- or dox-treated iAT2s in epithelial ducts of the EpiChip alongside HUVEC engineered vessels [Fig. 4(a)]. While DMSO-treated iAT2s had minimal effect on vascular morphology, co-culture of dox-treated iAT2s resulted in a significant disruption of vascular phenotype, with a significant increase in number of endothelial sprouts and vessel diameter, both changes known to be characteristic traits of tumor angiogenesis [Figs. 4(b)–4(d)].[43] Importantly, culture of engineered vessels alone with either dox or DMSO (but no iAT2s) had no effect on vessel morphology, suggesting that the phenotypic changes observed in the co-culture model resulted from expression of KRAS^{G12D} in the iAT2s, rather than the effect of doxycycline itself [Fig. 2(d), supplementary material].

We speculated that this angiogenic vascular behavior might result from altered paracrine signaling between KRAS^{G12D} expressing iAT2s and endothelial cells. To identify potential paracrine mediators promoting this change, we quantified the relative levels of angiogenic factors secreted into conditioned media from DMSO vs dox-treated BU3 NGST-TetOn:KRASG12D iAT2s. The ten factors most significantly upregulated in conditioned medium from the Dox-treated iAT2s are summarized in Fig. 4(e), and the full dataset can be found in Fig. 3, supplementary material. sVEGFR2 was identified as the most highly enriched protein in the KRAS^{G12D} conditioned media, however, given its role as a soluble decoy receptor for VEGFA, reducing the effective concentration of VEGFA seen by nearby endothelial cells, it is considered an anti-angiogenic molecule and was not investigated further. The second most highly upregulated factor detected in the screen was the urokinase-type plasminogen activator receptor (uPAR), a cell surface receptor tethered to the membrane via a cleavable GPI-anchor. Cleavage of this anchor allows uPAR to diffuse away from the cell as a paracrine signaling molecule known as soluble uPAR (suPAR).[44] suPAR has been previously implicated in driving increased angiogenesis both *in vitro* and *in vivo* and has been suggested as a biomarker that correlates with poor overall survival in non-small cell lung cancer patients.[45–48]

To investigate the association of KRAS mutations with expression of uPAR, genomic data from patients with LUAD generated as part of The Cancer Genome Atlas were analyzed. Comparison of expression of *PLAUR*, the gene encoding uPAR, in patients with a missense KRAS mutation at the G12 residue (including KRAS^{G12C} and KRAS^{G12D}) and without a KRAS^{G12} missense mutation revealed that tumors from patients with KRAS^{G12} mutations have increased expression of *PLAUR*. This suggests a functional association between KRAS^{G12} mutations and uPAR expression, raising the possibility that this soluble mediator may drive some of the angiogenic response seen in our model [Fig. 4(f)].[28,49–51] Hence, we next investigated the potential angiogenic role of suPAR in the KRAS^{G12D} context.

To test the role of suPAR in driving the observed vascular changes, we infused recombinant uPAR into an un-seeded epithelial duct to permit diffusion to HUVEC-seeded endothelial vessels in the EpiChip [Fig. 4(g)]. Vessels cultured in CKDCI++ and exposed to a suPAR gradient (30 ng/mL) displayed significantly increased diameter and number of endothelial sprouts as compared to vessels cultured in the EpiChip with CKDCI++ and vehicle alone, suggesting that suPAR is capable of phenocopying some of the elements of the angiogenic response seen in the co-culture of KRAS^{G12D} expressing iAT2s with HUVEC endothelium [Figs. 4(h)–4(j)].

III. DISCUSSION

Organ-on-a-chip models often combine multiple tissue types into a single platform and in a specified orientation to mimic the biologically relevant structure–function relationships of native tissues. They are particularly useful for bottom-up modeling of physiological processes and pathology, as they permit the development of more physiologically relevant organ- or tissue-specific cellular morphologies and behaviors than can be found in more traditional 2D or 3D monoculture. They also permit the observation of key morphologic events and cell–cell interactions with high spatiotemporal resolution that can enable detailed mechanistic studies of both normal and disease states.[52–57] Here, we focused on engineering a model of lung epithelial–endothelial crosstalk by seeding iPSC-derived AT2s into 3D blunt ended ducts of relevant alveolar size (~200 μm[58]) adjacent to engineered vessels composed of human endothelial cell-lined channels.[25,26,33] The iAT2s maintain their AT2 phenotype in this model despite the slightly softer than physiologic stiffness of native lung tissue (139 Pa vs approximately 500 Pa of native lung tissue).[59] Taken together, our results indicate this engineered platform facilitates modeling of paracrine crosstalk between our previously published epithelial-only human alveolar organoid model and vascular endothelium, which ultimately facilitated identification and validation of a pro-angiogenic paracrine signaling factor selectively expressed in KRAS G12D mediated LUAD.[26] Identification of such signaling changes is the first step toward targeted therapy for patients harboring such a mutation.

Cultures of single cell lineages typically utilize unique media formulations distinct to each cultured cell type. This represents a significant hurdle for investigators wishing to combine separately derived

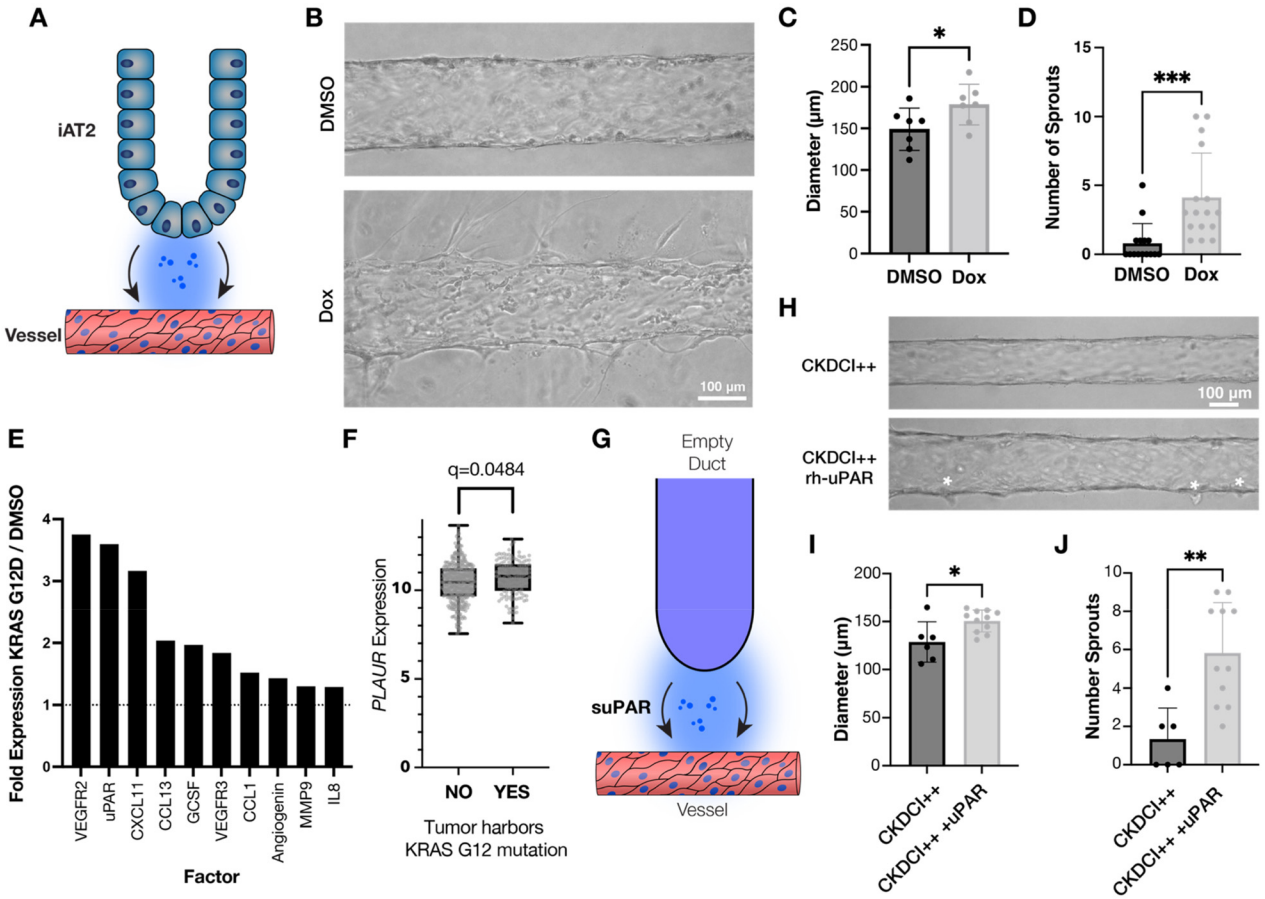

FIG. 4. Co-culture of duct harboring KRAS^{G12D}-expressing cells with adjacent vessel drives an angiogenic response that is mediated in part by epithelium-secreted suPAR or added suPAR. (a) Schematic depicting paracrine signaling between KRAS^{G12D} expressing iAT2s and adjacent endothelial vessel in the EpiChip (b) Representative images of HUVEC endothelial vessels co-cultured alongside DMSO or dox-treated KRAS^{G12D} iAT2s for 5 days. (c) and (d) Quantification of ductal diameters (c) in vessels co-cultured alongside DMSO or dox-treated KRAS^{G12D} iAT2 epithelial ducts and number of sprouts (d) after 5 days of co-culture. (e) Top 10 upregulated proteins found in media conditioned by dox-treated iAT2 cells, as compared to media conditioned by DMSO-treated iAT2 cells. (f) Comparison of *PLAUR* expression in LUAD patients with tumors harboring KRAS G12 mutations and those without. FDR computed using cBioPortal. (g) Schematic depicting experiment to test the role of the factors identified in (e) on vascular phenotype, where factors are introduced into an unseeded epithelial duct and diffuse toward the HUVEC endothelial vessel in the EpiChip. (h) Representative images of HUVEC vessels co-cultured for 5d alongside epithelial ducts supplemented with CKDCI++ alone or CKDCI++ with 30 ng/ml uPAR. (i) and (j) Quantification of average ductal diameter (i) and number of sprouts (j) for HUVEC ducts cultured alongside either CKDCI++ alone or CKDCI++ with intra-epithelial-duct infused uPAR. (* $p < 0.05$, ** $p < 0.01$, *** $p < 0.001$).

primary or iPSC-derived lineages in a single, common medium that will successfully maintain the phenotype and viability of each lineage in a co-culture. Here, we first developed a common serum-free, feeder-free defined medium able to support the co-existence of both iPSC-derived alveolar epithelial type 2 cells (iAT2s) and human umbilical vein endothelial cells (HUVECs). These lineages were co-cultured in a shared three-dimensional extracellular matrix and common medium containing factors critical for both epithelial and endothelial cell survival, and neither epithelial nor endothelial cell behavior was significantly altered from that in monoculture with their individualized, optimal media. Identification of the role of these growth factors in maintaining viability of both cell types raises the possibility that future endothelial cell-compatible media could be generated by supplementing native, defined stem cell media with these vascular-supporting factors.

Applying our new model to interrogate multicellular changes that might be associated with early stages of LUAD formation, we demonstrated that iAT2s overexpressing oncogenic KRAS^{G12D} displayed abnormal multi-layered, multi-luminal morphology in the EpiChip device and that endothelial cells co-cultured with these iAT2 KRAS^{G12D} mutants displayed increased angiogenic behaviors. We found that delivery of recombinant soluble uPAR is sufficient to phenocopy elements of the KRAS^{G12D}-mediated angiogenic response, altogether establishing a model of lung adenocarcinoma that allows for multicellular interrogation and investigation of mutation-specific paracrine signaling changes underlying tumor progression.

It is well established that paracrine signaling between tumor cells and nearby stromal cells are essential for cancer progression.[60,61] Given the significant role of endothelial cells in tumor progression, including angiocrine signaling and angiogenic response, there is a need

to develop models that facilitate investigation of the epithelial–endothelial crosstalk in diseases, such as LUAD.[62–64] In lung adenocarcinoma, the oncogenic $KRAS^{G12D}$ mutation in alveolar epithelial type 2 cells (AT2s) causes a loss of mature lineage identity genes such as surfactant protein C (*SFTPC*) and drives epithelial hyperplasia.[29,65] Our data corroborate these prior results, as the epithelium expressing the oncogenic $KRAS^{G12D}$ mutation shows morphological changes consistent with a hyperproliferative, immature phenotype, while also identifying that co-culture of these mutant iAT2s with a normal endothelium elicits an angiogenic response, reminiscent of a tumor phenotype.

The angiogenic mediator uPAR has been suggested to play a role in endothelial cell migration.[45,66–69] While the precise role of uPAR in tumor angiogenesis is unclear, it has been shown that increased expression levels of uPAR in patients with non-small cell lung cancer is associated with poor overall survival, and uPAR over-expression in non-small cell lung cancer cell lines was found to be functionally associated with RAS mutations.[49,70] Consistent with these previously published findings, our analysis of conditioned medium from $KRAS^{G12D}$-induced iAT2s identified soluble VEGFR2 (sVEGFR2) and soluble uPAR (suPAR) as the two most highly enriched factors in the $KRAS^{G12D}$ iAT2 conditioned medium. In our model, treatment of endothelial cells with recombinant uPAR significantly increased vessel diameter and sprouting, highlighting the role of this factor in $KRAS^{G12D}$-mediated angiogenesis and further supporting the pro-angiogenic nature of soluble uPAR. These findings suggest that uPAR may be an actionable target to limit tumor angiogenesis in LUAD patients harboring a $KRAS^{G12D}$ mutation.

The lung-on-a-chip platform reported here is a highly adaptable platform that permits mechanistic investigation into the origins of lung adenocarcinoma with high spatiotemporal precision. $KRAS^{G12D}$ is only one of several common and recurring mutations detected in patients with LUAD, and the modeling of additional common LUAD driver mutations, such as $EGFR^{L858R}$, a constitutively active EGFR receptor, requires only re-engineering of the iAT2 cell line to reflect these cancer-specific genomic changes. These mutations may show distinct epithelial morphologies and drive unique, mutation-specific responses in the adjacent endothelial vessel. Additionally, the distance between the epithelium and the endothelium warrants further study and customization, as additional behaviors could potentially emerge as the two compartments come closer together. For example, close proximity of epithelium and endothelium would be required to study highly labile factors (such as nitric oxide) or the interactions triggered by mechanical stresses transmitted across the collagen matrix (e.g., tension driven matrix alignment). These potential interactions would need to be examined in future studies when our ability to bring these compartments closer together becomes technically feasible. Further improvements to the model, including the development of an in-device air-liquid interface for AT2 culture or mechanical actuation of the hydrogel, could leverage some of the biological insights gleaned from other lung-on-a-chip models to further improve the biological relevance of our model and provide enhanced mechanistic insight. Overall, this study adds to the growing field of reductionist organotypic models of cancer that enable a more nuanced and physiologically relevant investigation of oncogenesis than is possible in 2D culture and complements the more costly and biologically complex *in vivo* models of disease.

IV. CONCLUSION

In this work, we developed and validated a novel lung-on-a-chip device that permits the co-culture of iPSC-derived alveolar epithelial type 2 cells with HUVEC endothelium. Using this device, we demonstrate that $KRAS^{G12D}$, a common driver mutation in lung adenocarcinoma, leads to epithelia that resist growth arrest, producing hypercellular ducts with reduced luminal volume, and secrete angiogenic factors—including suPAR—which affect the neighboring endothelium. This biological insight suggests that targeting suPAR in patients with $KRAS^{G12D}$-driven LUAD may have therapeutic benefit.

V. METHODS

A. Cell culture

Induced pluripotent stem cell (iPSC)-derived alveolar epithelial type 2 cells (iAT2s) were generated as previously described.[26,33] Briefly, iPSCs—BU3 $NKX2\text{-}1^{GFP}$ $SFTPC^{tdTomato}$ (NGST) and SPC2 [clone $SPC2\text{-}SFTPC^{tdTomato}$(ST)-B2]—were taken through the directed differentiation protocol, sorted for $NKX2\text{-}1^{GFP}+$ or $CD47^{hi}/CD26^{lo}$ cells at day 15 of differentiation, respectively, and further sorted for $SFTPC^{tdTomato}+$ cells at day 45 of differentiation. Putative iAT2s were cultured in feeder-free conditions ("CKDCI" media: CHIR, KGF, Dexamethasone, 8-Br cAMP, IBMX)[26] in 3D Matrigel (Corning) droplets, and passaged every 10–14 days.

For induction of LUAD-associated gene mutations in iAT2s, we used a previously published iPSC subclone of the above-mentioned BU3 NGST line, which has been gene edited to carry a doxycycline-inducible $KRAS^{G12D}$ oncogenic mutant cDNA, bi-allelically targeted to the "safe harbor" AAVS1 locus (iPSC clone name "BU3 NGST-TetOn: KRASG12D," also known as "BU3 NGST KRAS3").[29] After directed differentiation of this clone into iAT2s (hereafter $KRAS^{G12D}$ iAT2s), doxycycline (dox; 1 μg/ml) or vehicle control (DMSO) were added to parallel wells of $KRAS^{G12D}$ iAT2s, and experiments were performed after approximately 3 months of dox and DMSO treatment.

Human umbilical vein endothelial cells (HUVECs, Lonza) were cultured in $EBM2^{TM}$ Basal Medium (Lonza) supplemented with an EGM2 bullet kit (Lonza). In co-culture in the microfluidic devices, HUVECs were cultured in CKDCI supplemented with VEGFA and bFGF to concentrations equivalent to those in EGM2 medium, creating a co-culture medium herein named "CKDCI++." All HUVECs were used before passage 8. All cells were cultured in a humidified incubator at 37 °C and 5% CO_2.

B. EpiChip device fabrication and seeding

EpiChip devices were fabricated similarly to previous work, with the notable exception of an increased epithelial duct seeding density necessary when seeding iAT2 to ensure adequate epithelial monolayer formation.[32] Briefly, polydimethylsiloxane (PDMS, Sylgard 184, Dow-Corning) was mixed with its curing agent in a 10:1 ratio, poured over microfabricated molds, and allowed to polymerize. Devices were then separated from the mold, bonded to glass using oxygen plasma and functionalized with 0.01% Poly-L-lysine and 1% glutaraldehyde (EMS). After three washes in DI water, 160 μm acupuncture needles (Seirin) were loaded into the gel region through the needle guides. Devices were UV sterilized for 15 min. A 2.5 mg/ml collagen solution was prepared as described previously and 35 μl of collagen solution was added to each device. This resulting collagen gel has a Young's modulus of 130 ± 39 Pa.[32]

The next day, needles were removed, forming the channels and ducts, and devices were chilled at 4 °C for 30 min. 75 μl of cold PBS with 1% Growth Factor Reduced Matrigel (Corning) was added to the epithelial port. Devices were rocked overnight at 4 °C, washed three times with cold PBS, and allowed to come to room temperature. HUVECs were resuspended in EGM2 at 1×10^6 cells/ml and seeded into the endothelial channel by adding 50 μl of cell solution to one endothelial port and 45 μl to the other. Cells were allowed to perfuse through the endothelial channel for 15 min before replacing the cell suspension with 90 μl of fresh EGM2 in each port. Devices were rocked along the endothelial axis. For these devices, the expected maximal volumetric flow rate is ~1.06 μl/s and maximal shear stress is ~3.3 dyn/cm^2.[32]

iAT2 spheroids were dissociated using Dispase (Corning) at 37 °C for 1 h, followed by 0.05% trypsin at 37 °C for 12 min. iAT2s were then resuspended in CKDCI + VEGFA + bFGF ("CKDCI++") + 10 μM Y27632 (SellekChem) at a concentration of 1×10^6 cells/ml. Both endothelial ports were emptied and replaced with 45 μl of CKDCI++ and 50 μl of iAT2s solution was added to the epithelial port. iAT2s were allowed to flow into the epithelial duct until an appropriate density was achieved under direct live microscopy visualization. As noted earlier, adequate seeding density for iAT2 cells was a dense monolayer, with cell–cell juxtaposition across the sides and top/bottom of the duct, without large regions (2–3 cell diameters) of acellularity, as has been previously described for seeding other cell types in this device. Once the critical density of cells in the epithelial duct was achieved, media in all ports was replaced with 90 μl of CKDCI++ and devices were cultured on a rocker in the incubator, rocking along their endothelial axis, for 5 days. Media was exchanged every 24 h. In experiments utilizing inducible cells, devices were cultured with doxycycline or DMSO supplementation.

C. Immunofluorescence

Devices were fixed in 4% paraformaldehyde (Electron Microscopy Sciences) in CKDCI++ for 30 min on a rocker in a humidified incubator. Devices were washed three times with PBS, permeabilized using 0.25% Triton-X in PBS for 30 min, washed three more times in PBS, and blocked overnight in 3% BSA in PBS (Sigma). Devices were incubated with primary antibody at the specified concentration on a rocker overnight at 4 °C. After three washes in PBS, devices were incubated with the appropriate secondary antibody (1:1000 dilution), again rocking overnight at 4 °C. During this overnight incubation, samples were additionally stained with DAPI (1:1000, Thermo) and phalloidin of an appropriate color (Alexa Fluor™ Plus, 1:1000; Thermo). After three more PBS washes, devices were imaged on a Leica SP8 laser scanning confocal microscope (Leica Microsystems) with Leica HC FLUOTAR L 25×/0.95 W VISIR controlled by LASX software. 2D monolayer images were collected using a Nikon Eclipse Ti2 outfitted with a 20× Nikon Plan Apo objective and an Evolve 512 camera (Photometrics).

Antibodies used for morphologic analysis included: EpCAM (CST #2929, mouse, 1:500 dilution), E-Cadherin (CST #3195, clone 24E10, rabbit, 1:500 dilution), anti-Pro-SP-B (Seven Hills Bioreagents, rabbit, 1:250), VE-Cadherin (Santa Cruz #9989, Clone F-8, mouse, 1:500), and Ki67 (Abcam, ab15580, rabbit, 1:500 dilution). All secondary antibodies used were Invitrogen Highly Cross-Adsorbed Secondary Antibodies, Alexa Fluor Plus (Thermo, used at 1:1000 dilution) targeted to the species of primary antibody with appropriate, non-overlapping colors selected.

D. Transmission electron microscopy

To prepare samples for transmission electron microscopy (TEM), devices were seeded and cultured for five days as previously described. Samples were fixed by perfusion with a mixture of 2% glutaraldehyde and 1% paraformaldehyde made fresh in a 0.1 M sodium cacodylate buffer (Sigma). After 90 min of fixation in this mixture at room temperature, samples were removed from the devices using a 5 mm biopsy punch, punching a hole around the epithelial duct, but being careful not to crack the cover glass below. Fixation continued for a total of 3 h. The glass coverslips were carefully removed, and samples were post fixed in 1% osmium, block stained with 1% uranyl acetate, then dehydrated and infiltrated with Epon resin mixed 1:1 with propyleneoxide using standard methods. The samples were embedded in upside down BEEM capsules with fixed collagen matrix oriented at the flat bottom. After overnight polymerization, the end opposite to the matrix was trimmed off, the PDMS extracted with a needle and the samples re-embedded in Embed 812 Resin (Electron Microscopy Sciences). 70 nm sections were cut and stained with 4% uranyl acetate and 0.2% lead citrate. Samples were then imaged on a Phillips CM12 TEM.

E. Proliferation analysis

To compare the proliferation of cells expressing the dox-induced $KRAS^{G12D}$ mutation to those treated with DMSO, iAT2s were seeded into the EpiChip and fixed one day and 3 days post seeding [Fig. 1(a)]. After permeabilization, cells were stained with a primary antibody targeting Ki67 (CST #12202, Rabbit, 1:500) and processed as described above. Upon imaging, the number of total nuclei and Ki67+ nuclei were manually counted, and the fraction of proliferating cells was quantified by dividing the number of Ki67+ nuclei by the total number of nuclei counted in that device.

F. Conditioned medium analysis

Conditioned medium was collected from either DMSO or dox-treated iAT2 cells in 3D alveolosphere culture. Two mL of supernatant was collected every 2 days, flash frozen, and stored at −80 °C. Once 10 ml of supernatant per condition were collected, samples were thawed on ice and pooled. Pooled samples were immediately applied to pre-activated membranes from the Angiogenesis C1000 Array (Raybiotech), and processing was performed according to the manufacturer's instructions. Comparison of relative protein content was analyzed as per kit instructions.

To test the angiogenic potential of uPAR, recombinant soluble uPAR (R&D 807-UK-100, 30 ng/ml) was delivered via an unseeded epithelial duct at a dose comparable to previously described levels of soluble uPAR secretion from tumors.[45] The angiogenic response of each vessel was assessed by quantifying changes in vessel diameter and number of sprouts, two factors known to be increased in tumor angiogenesis, in vessels exposed to soluble uPAR compared to vessels exposed to vehicle alone. To quantify vessel diameter, vessels were measured at three equally spaced regions along the length of the vessel using FIJI, and the diameter was reported as the average of those measurements. To quantify the number of sprouts, each vessel was

visualized and endothelial cells abluminal to the plane of the monolayer were counted as spouting cells.

G. TCGA gene expression analysis

A LUAD-specific TCGA dataset was mined using cBioPortal to compare expression levels of *PLAUR*, the gene encoding uPAR, in patients with tumors harboring a KRAS G12 missense mutation to patients without KRAS G12 missense mutations.[49–51] All G12 missense mutations were analyzed as the dataset was not sufficiently enriched in G12D samples (20 patients of 566) for G12D-specific analysis of PLAUR expression. Data were replotted using GraphPad Prism. Statistics, including FDR, computed using cBioPortal analysis tools.

H. Statistics and plotting

All statistics and plotting of graphs and charts was performed in Prism (GraphPad). Unless otherwise specified, for two group analyses, a Student's t-test was performed, while a one-way ANOVA analysis with Tukey post-hoc analysis was performed for multi-group comparisons.

SUPPLEMENTARY MATERIAL

See the supplementary material for three additional supplementary material referenced in the text, including additional information about development of the iAT2 epithelial duct (supplementary material Fig. 1), further morphological characterization of each duct (supplementary material Fig. 2), and for comparison of the angiogenic factor content of the conditioned medium (supplementary material Fig. 3).

ACKNOWLEDGMENTS

This work was funded by NIH Grant Nos. R01HL095993 and N01 75N92020C00005 to D.N.K., the NSF Science and Technology Center for Engineering Mechanobiology (No. CMMI-1548571), and a Boston University Kilachand Multicellular Design Program Accelerator Grant and an Allen Distinguished Investigator grant from the Paul G. Allen Family Foundation to C.S.C. and D.N.K. K.A.G. acknowledges the support from the NIH through the Biology of the Lung: A Multidisciplinary Program (NIH T32 HL007035). J.H. acknowledges the support from Boston University Kilachand Multicellular Design Program Postdoctoral Fellowship.

The results shown here are in part based upon data generated by the TCGA Research Network: https://www.cancer.gov/tcga.

AUTHOR DECLARATIONS

Conflict of Interest

C.S.C. is a founder and owns shares of Innolign Biomedical, a company that is developing engineered organ models for pharmaceutical research and development, and Satellite Biosciences, a company that is developing cell-based therapies. The other authors declare that they have no competing interest.

Ethics Approval

Ethics approval is not required.

Author Contributions

Keith A. Gagnon and Jessie Huang contributed equally to this work.

Keith A. Gagnon: Conceptualization (equal); Formal analysis (equal); Investigation (equal); Methodology (equal); Visualization (equal); Writing – original draft (equal); Writing – review & editing (equal). **Jessie Huang:** Conceptualization (equal); Data curation (equal); Formal analysis (equal); Funding acquisition (equal); Investigation (equal); Methodology (equal); Visualization (equal); Writing – original draft (equal); Writing – review & editing (equal). **Olivia T. Hix:** Investigation (supporting); Writing – review & editing (supporting). **Veronica W. Hui:** Investigation (supporting); Writing – review & editing (supporting). **Anne Hinds:** Investigation (supporting); Methodology (supporting); Writing – review & editing (supporting). **Esther Bullitt:** Investigation (supporting); Writing – review & editing (supporting). **Jeroen Eyckmans:** Methodology (supporting); Writing – review & editing (supporting). **Darrell N. Kotton:** Conceptualization (equal); Funding acquisition (equal); Project administration (equal); Supervision (equal); Writing – review & editing (equal). **Christopher S. Chen:** Conceptualization (equal); Funding acquisition (equal); Project administration (equal); Supervision (equal); Writing – review & editing (equal).

DATA AVAILABILITY

The data that support the findings of this study are available from the corresponding authors upon reasonable request.

REFERENCES

[1]R. L. Siegel, K. D. Miller, N. S. Wagle, and A. Jemal, "Cancer statistics, 2023," Ca-Cancer J. Clin. **73**, 17–48 (2023).
[2]T. V. Denisenko, I. N. Budkevich, and B. Zhivotovsky, "Cell death-based treatment of lung adenocarcinoma," Cell Death Dis. **9**, 117 (2018).
[3]X. Xu *et al.*, "Evidence for type II cells as cells of origin of K-Ras–induced distal lung adenocarcinoma," Proc. Natl. Acad. Sci. U. S. A. **109**, 4910–4915 (2012).
[4]T. J. Desai, D. G. Brownfield, and M. A. Krasnow, "Alveolar progenitor and stem cells in lung development, renewal and cancer," Nature **507**, 190–194 (2014).
[5]K.-D. Alysandratos *et al.*, "Culture impact on the transcriptomic programs of primary and iPSC-derived human alveolar type 2 cells," JCI Insight **8**, e158937 (2023).
[6]C. D. Foster, L. S. Varghese, R. B. Skalina, L. W. Gonzales, and S. H. Guttentag, "*In vitro* transdifferentiation of human fetal type II cells toward a type I–like cell," Pediatr. Res. **61**, 404–409 (2007).
[7]P. S. Hiemstra, T. D. Tetley, and S. M. Janes, "Airway and alveolar epithelial cells in culture," Eur. Respir. J. **54**, 1900742 (2019).
[8]D. Huh *et al.*, "Reconstituting organ-level lung functions on a chip," Science **328**, 1662–1668 (2010).
[9]B. A. Hassell *et al.*, "Human organ chip models recapitulate orthotopic lung cancer growth, therapeutic responses, and tumor dormancy in vitro," Cell Rep. **21**, 508–516 (2017).
[10]M. Felder *et al.*, "Impaired wound healing of alveolar lung epithelial cells in a breathing lung-on-a-chip," Front. Bioeng. Biotechnol. **7**, 3 (2019).
[11]A. O. Stucki *et al.*, "A lung-on-a-chip array with an integrated bio-inspired respiration mechanism," Lab Chip **15**, 1302–1310 (2015).
[12]K. L. Sellgren, E. J. Butala, B. P. Gilmour, S. H. Randell, and S. Grego, "A biomimetic multicellular model of the airways using primary human cells," Lab Chip **14**, 3349–3358 (2014).
[13]X. Yang *et al.*, "Nanofiber membrane supported lung-on-a-chip microdevice for anti-cancer drug testing," Lab Chip **18**, 486–495 (2018).

[14]W. Bertrams *et al.*, "Transcriptomic comparison of primary human lung cells with lung tissue samples and the human A549 lung cell line highlights cell type specific responses during infections with influenza A virus," Sci. Rep. **12**, 20608 (2022).
[15]S. Ferreira Lopes *et al.*, "Primary and immortalized human respiratory cells display different patterns of cytotoxicity and cytokine release upon exposure to deoxynivalenol, nivalenol and fusarenon-X," Toxins **9**, 337 (2017).
[16]R. J. Swain, S. J. Kemp, P. Goldstraw, T. D. Tetley, and M. M. Stevens, "Assessment of cell line models of primary human cells by Raman spectral phenotyping," Biophys. J. **98**, 1703–1711 (2010).
[17]R. J. Mason and M. C. Williams, "Phospholipid composition and ultrastructure of A549 cells and other cultured pulmonary epithelial cells of presumed type II cell origin," Biochim. Biophys. Acta **617**, 36–50 (1980).
[18]D. E. Discher, P. Janmey, and Y. L. Wang, "Tissue cells feel and respond to the stiffness of their substrate," Science **310**, 1139–1143 (2005).
[19]M. J. Paszek and V. M. Weaver, "The tension mounts: Mechanics meets morphogenesis and malignancy," J. Mammary Gland Biol. Neoplasia **9**, 325–342 (2004).
[20]K. Wolf and P. Friedl, "Extracellular matrix determinants of proteolytic and non-proteolytic cell migration," Trends Cell Biol. **21**, 736–744 (2011).
[21]D. Baptista, L. Teixeira, C. van Blitterswijk, S. Giselbrecht, and R. Truckenmüller, "Overlooked? Underestimated? Effects of substrate curvature on cell behavior," Trends Biotechnol. **37**, 838–854 (2019).
[22]L. Knudsen and M. Ochs, "The micromechanics of lung alveoli: Structure and function of surfactant and tissue components," Histochem. Cell Biol. **150**, 661–676 (2018).
[23]M. Luciano *et al.*, "Cell monolayers sense curvature by exploiting active mechanics and nuclear mechanoadaptation," Nat. Phys. **17**, 1382–1390 (2021).
[24]A. Yu *et al.*, "Reconstructing codependent cellular cross-talk in lung adenocarcinoma using REMI," Sci. Adv. **8**, eabi4757 (2022).
[25]K. Hurley *et al.*, "Reconstructed single-cell fate trajectories define lineage plasticity windows during differentiation of human PSC-derived distal lung progenitors," Cell Stem Cell **26**, 593–608 (2020).
[26]A. Jacob *et al.*, "Differentiation of human pluripotent stem cells into functional lung alveolar epithelial cells," Cell Stem Cell **21**, 472–488 (2017).
[27]S. Devarakonda, D. Morgensztern, and R. Govindan, "Genomic alterations in lung adenocarcinoma," Lancet Oncol. **16**, e342–e351 (2015).
[28]The Cancer Genome Atlas Research Network, "Comprehensive molecular profiling of lung adenocarcinoma," Nature **511**, 543 (2014).
[29]A. F. M. Dost *et al.*, "Organoids model transcriptional hallmarks of oncogenic KRAS activation in lung epithelial progenitor cells," Cell Stem Cell **27**, 663–678 (2020).
[30]M. N. Zeissig, L. M. Ashwood, O. Kondrashova, and K. D. Sutherland, "Next batter up! Targeting cancers with KRAS-G12D mutations," Trends Cancer **9**, 955–967 (2023).
[31]B. Ricciuti *et al.*, "Dissecting the clinicopathologic, genomic, and immunophenotypic correlates of $KRAS^{G12D}$-mutated non-small-cell lung cancer," Ann. Oncol. **33**, 1029–1040 (2022).
[32]M. L. Kutys *et al.*, "Uncovering mutation-specific morphogenic phenotypes and paracrine-mediated vessel dysfunction in a biomimetic vascularized mammary duct platform," Nat. Commun. **11**, 3377 (2020).
[33]A. Jacob *et al.*, "Derivation of self-renewing lung alveolar epithelial type II cells from human pluripotent stem cells," Nat. Protoc. **14**, 3303–3332 (2019).
[34]F. Brasch *et al.*, "Surfactant protein B in type II pneumocytes and intra-alveolar surfactant forms of human lungs," Am. J. Respir. Cell Mol. Biol. **30**, 449–458 (2004).
[35]C. E. Barkauskas *et al.*, "Type 2 alveolar cells are stem cells in adult lung," J. Clin. Invest. **123**, 3025–3036 (2013).
[36]T. A. Spanholtz *et al.*, "Vascular endothelial growth factor ($VEGF^{165}$) plus basic fibroblast growth factor (bFGF) producing cells induce a mature and stable vascular network—A future therapy for ischemically challenged tissue," J. Surg. Res. **171**, 329–338 (2011).
[37]K. Bindewald *et al.*, "Opposite effect of cAMP signaling in endothelial barriers of different origin," Am. J. Physiol. Cell Physiol. **287**, C1246–55 (2004).
[38]K. L. Bryant, J. D. Mancias, A. C. Kimmelman, and C. J. Der, "KRAS: feeding pancreatic cancer proliferation," Trends Biochem. Sci. **39**, 91–100 (2014).
[39]X. Liu, M. Jakubowski, and J. L. Hunt, "*KRAS* gene mutation in colorectal cancer is correlated with increased proliferation and spontaneous apoptosis," Am. J. Clin. Pathol. **135**, 245–252 (2011).
[40]Y. Mao, S. Sun, and K. D. Irvine, "Role and regulation of Yap in $Kras^{G12D}$-induced lung cancer," Oncotarget **8**, 110877–110889 (2017).
[41]E. L. Jackson *et al.*, "Analysis of lung tumor initiation and progression using conditional expression of oncogenic K-*ras*," Genes Dev. **15**, 3243–3248 (2001).
[42]D. Hanahan and R. A. Weinberg, "Hallmarks of cancer: The next generation," Cell **144**, 646–674 (2011).
[43]S. M. Weis and D. A. Cheresh, "Tumor angiogenesis: Molecular pathways and therapeutic targets," Nat. Med. **17**, 1359–1370 (2011).
[44]H. W. Smith and C. J. Marshall, "Regulation of cell signalling by uPAR," Nat. Rev. Mol. Cell Biol. **11**, 23–36 (2010).
[45]J. S. Rao, M. Gujrati, and C. Chetty, "Tumor-associated soluble uPAR-directed endothelial cell motility and tumor angiogenesis," Oncogenesis **2**, e53 (2013).
[46]J. J. Lu *et al.*, "Prognostic value of urokinase plasminogen activator system in non-small cell lung cancer: A systematic review and meta-analysis," Mol. Clin. Oncol. **8**, 127–132 (2018).
[47]S. Herkenne *et al.*, "The interaction of uPAR with VEGFR2 promotes VEGF-induced angiogenesis," Sci. Signal. **8**, ra117 (2015).
[48]G. Marone, F. Borriello, G. Varricchi, A. Genovese, and F. Granata, "Basophils: Historical reflections and perspectives," Chem. Immunol. Allergy **100**, 172–192 (2014).
[49]E. Cerami *et al.*, "The cBio cancer genomics portal: An open platform for exploring multidimensional cancer genomics data," Cancer Discovery **2**, 401–404 (2012).
[50]J. Gao *et al.*, "Integrative analysis of complex cancer genomics and clinical profiles using the cBioPortal," Sci. Signal. **6**, pl1 (2013).
[51]I. de Bruijn *et al.*, "Analysis and visualization of longitudinal genomic and clinical data from the AACR project GENIE biopharma collaborative in cBioPortal," Cancer Res. **83**, 3861–3867 (2023).
[52]D. E. Ingber, "Human organs-on-chips for disease modelling, drug development and personalized medicine," Nat. Rev. Genet. **23**, 467–491 (2022).
[53]C. M. Leung *et al.*, "A guide to the organ-on-a-chip," Nat. Rev. Methods Primers **2**, 33 (2022).
[54]D. Antoni, H. Burckel, E. Josset, and G. Noel, "Three-dimensional cell culture: A breakthrough in vivo," Int. J. Mol. Sci. **16**, 5517–5527 (2015).
[55]C. Jensen and Y. Teng, "Is it time to start transitioning from 2D to 3D cell culture?," Front. Mol. Biosci. **7**, 33 (2020).
[56]M. Kapałczyńska *et al.*, "2D and 3D cell cultures—A comparison of different types of cancer cell cultures," Arch. Med. Sci. **14**, 910–919 (2018).
[57]D. van Berlo *et al.*, "Stem cells, organoids, and organ-on-a-chip models for personalized *in vitro* drug testing," Curr. Opin. Toxicol. **28**, 7–14 (2021).
[58]M. Ochs *et al.*, "The number of alveoli in the human lung," Am. J. Respir. Crit. Care Med. **169**, 120–124 (2004).
[59]F. Liu *et al.*, "Feedback amplification of fibrosis through matrix stiffening and COX-2 suppression," J. Cell Biol. **190**, 693–706 (2010).
[60]R. M. Bremnes *et al.*, "The role of tumor stroma in cancer progression and prognosis: Emphasis on carcinoma-associated fibroblasts and non-small cell lung cancer," J. Thorac. Oncol. **6**, 209–217 (2011).
[61]T. D. Tlsty and L. M. Coussens, "Tumor stroma and regulation of cancer development," Annu. Rev. Pathol. **1**, 119–150 (2006).
[62]G. Bergers and L. E. Benjamin, "Tumorigenesis and the angiogenic switch," Nat. Rev. Cancer **3**, 401–410 (2003).
[63]M. Singhal and H. G. Augustin, "Beyond angiogenesis: Exploiting angiocrine factors to restrict tumor progression and metastasis," Cancer Res. **80**, 659–662 (2020).
[64]V. O. Oria and J. T. Erler, "Tumor angiocrine signaling: Novel targeting opportunity in cancer," Cells **12**, 2510 (2023).
[65]K. D. Sutherland *et al.*, "Multiple cells-of-origin of mutant K-Ras-induced mouse lung adenocarcinoma," Proc. Natl. Acad. Sci. U. S. A. **111**, 4952–4957 (2014).
[66]K. Bifulco *et al.*, "The soluble form of urokinase receptor promotes angiogenesis through its Ser^{88}-Arg-Ser-Arg-Tyr^{92} chemotactic sequence," J. Thromb. Haemostasis **8**, 2789–2799 (2010).

[67]B. Gorantla, S. Asuthkar, J. S. Rao, J. Patel, and C. S. Gondi, "Suppression of the uPAR–uPA system retards angiogenesis, invasion, and *in vivo* tumor development in pancreatic cancer cells," Mol. Cancer Res. **9**, 377–389 (2011).
[68]E. Hugdahl, I. M. Bachmann, C. Schuster, R. G. Ladstein, and L. A. Akslen, "Prognostic value of uPAR expression and angiogenesis in primary and metastatic melanoma," PLoS One **14**, e0210399 (2019).
[69]H. Raghu *et al.*, "Suppression of uPA and uPAR attenuates angiogenin mediated angiogenesis in endothelial and glioblastoma cell lines," PLoS One **5**, e12458 (2010).
[70]C. D. Mauro *et al.*, "Urokinase-type plasminogen activator receptor (uPAR) expression enhances invasion and metastasis in RAS mutated tumors," Sci. Rep. **7**, 9388 (2017).